Energy & Buildings 169 (2018) 185–194

Contents lists available at ScienceDirect

Energy & Buildings

journal homepage: www.elsevier.com/locate/enbuild

# A new ventilated window with PCM heat exchanger—Performance analysis and design optimization

Yue Hu*, Per Kvols Heiselberg

*Department of Civil Engineering, Aalborg University, Thomas Manns Vej 23, Aalborg 9220, Denmark*

ARTICLE INFO

*Article history:*
Received 23 January 2018
Revised 21 March 2018
Accepted 22 March 2018
Available online 29 March 2018

*Keywords:*
Phase change material
Ventilated window
Ventilation pretreatment
PCM modeling

ABSTRACT

This paper proposes a ventilated window with a phase change material (PCM) heat exchanger as a new window application. In summer, night ventilation mode is operated to discharge energy stored in PCM by the ambient cold air, which can be reloaded again, when ventilation pre-cooled air is provided.

Numerical model is built and verified by full-scale experiment to evaluate the PCM ventilation system. The nonlinear properties and hysteresis of PCM are set in the model. The conclusion is that the configuration optimization should be based on different climates. In the case study in Copenhagen, the heat exchanger with 10 mm plate thickness is optimized. It can cool down the ventilated air 6.5 °C on average in 3.9 h pre-cooling effective time with 3.19 MJ/day energy saving. The material cost saving is 16.87% compared to 20 mm plate thickness which has similar discharged heat amount. Nevertheless, the heat exchanger with 5 mm plate thickness has a faster thermal response and a higher cost saving ability, which is good for the climate when the period of outdoor air temperature suitable for night ventilation in a day is short.



## 1. Introduction

Renewable energy has been used in low energy buildings and other building applications to cut down the building energy consumption for a sustainable building environment. This kind of energy is mostly intermittent and highly depends on the outdoor climate, such as solar energy. A thermal energy storage (TES) system is a promising way to improve the efficiency of solar energy applications. Phase change material (PCM) is a good candidate for TES because of its thermal properties, such as high latent heat and isothermal heat transfer process. Moreover, the physical properties of PCM make it easy to integrate into building elements. Therefore, it has gained a large interest in research and building market recently [1].

PCM is different from other materials in the way that it can absorb or release a large amount of latent heat when changing phase [2]. The energy density of the material is relatively high so that the volume of the system could be smaller in comparison with other TES. In addition, the temperature of PCM will stay almost constant in the phase change period, which means the surface temperature of building envelope will not be too high, thus avoiding a high heat transfer [3]. Organic PCMs are drawing much attention because they have high latent heat capacity and stable physical and chemical properties [4]. Moreover, for some of them, the transition temperature is in the thermal comfort range of human body, which makes them good candidates to combine with air conditioning systems, ventilation systems as well as building envelopes [5].

PCM has been used in many building applications for thermal storage and thermal control. One of the applications is mixing PCM with building material for building constructions, such as gypsum board, plaster, concrete or other wall boards. It can also be a component like blind and layer for ceiling and wall. Michal et al. [6] mixed PCM with concrete and built a hollow concrete deck. The thermal properties of the new concrete construction were numerically and experimentally studied and compared with other materials. The results showed that there is an energy-saving potential for mixing PCM in concrete constructions. Active PCM applications include applying PCM in air conditioning system, ventilation façade, etc. Diarce et al. [7] studied the thermal properties of an actively ventilated façade with PCM board in the outer layer. The study compared the thermal behavior of the system with traditional constructions by modeling in Design Builder. The results showed that the thermal storage increases greatly in the phase change process of PCM, which decreased the chance of overheating for the envelope. Alvaro et al. [8] studied the thermal performance of a ventilated façade with macro encapsulated PCM in its air cavity. The results showed that with night ventilation, the system could greatly reduce the cooling load. Hicham et al. [9,10] built and tested a double-layer window with PCM shading device in the

* Corresponding author.
*E-mail address:* hy@civil.aau.dk (Y. Hu).

https://doi.org/10.1016/j.enbuild.2018.03.060
0378-7788/

middle of glazing layers. The results showed that the PCM shading device decreases the U value of the window.

The main drawback of PCM is its low thermal conductivity [11]. The heat is absorbed by the surface layer of PCM but is blocked due to the low thermal conductivity, which results in a long time for the melting procedure. Consequently, the thickness of PCM implementations should be within a certain limited range. Another drawback of PCM is its thermal expansion. The volume expansion of paraffin wax is in the order of 10% volume change [12,13], which is similar to the inorganic PCM, but smaller forces as paraffin wax is softer [13]. In this paper the PCM used is paraffin wax 22, which has a phase change temperature at 22 °C. The PCM is absorbed by fiber board (50% PCM and 50% fiber). The soft texture and air voids in the fiber board make the expansion possible. Moreover, the temperature change range of PCM in night ventilation application is smaller than the ones tested in the above literature, so the expansion of PCM is less considered in this work.

An accurate numerical model for PCM applications is necessary in order to give guidance for the engineering optimization and architectural design. However, the nonlinear properties of PCM make it difficult for the modeling [14]. For example, the heat capacity, enthalpy, viscosity and thermal conductivity could be dependent on temperature, and the heat capacity as a function of temperature is different in the freezing and melting processes because of the hysteresis effect. For organic PCM, there is also the problem of purification of the material, which makes the properties more complicated. For nonorganic PCM, there are problems such as supercooling effect, phase segregation, unstable thermal and chemical composition [15]. Those phenomena were considered in some experimental works [16–18], but the ideal or average heat capacity was used and the hysteresis was ignored in most of the modeling and numerical works [19–23].

Some other software such as COMSOL Multiphysics or FEMLAB (the predecessor of COMSOL) have been used to solve the numerical problems in relation to PCM. COMSOL Multiphysics is good at solving multi-physics problems and modeling complicated and irregular components with non-linear properties. A conduction heat transfer model in COMSOL using the DSC measured non-linear heat capacity was verified by data from experiment [18]. The temperature in the center of the PCM plate from the experiment was compared to the numerical model. The result showed a good consistency. Another study was about modeling of an innovative honeycomb wallboard in COMSOL using fictive heat capacity from DSC measurement [24]. The model showed good agreement with the experimental results. A similar model for a PCM storage facility was built in COMSOL Multiphysics using two different approximation methods for heat capacity. The results showed that both the effective heat capacity method and the enthalpy method are good at estimating the heat transfer process [25].

This paper proposes a new ventilated window with a PCM heat exchanger and analyzes the system performance in summer. A finite model considering nonlinear properties and hysteresis of PCM is built in COMSOL Multiphysics to simulate the heat transfer in the heat exchanger, and is verified by full-scale laboratory experiment. The model is used to study the thermal behavior of the system in night ventilation mode and ventilation air pre-cooling mode, as well as to estimate the energy saving potential when precooling the ventilated air in cases in Copenhagen.

## 2. System performance analysis

Fig. 1 illustrates a normal room with a ventilated window. A heat exchanger made of PCM plates is integrated with the ventilated window to precool the ventilated air, the overview of the PCM heat exchanger and plates can be seen in Fig. 7. The ventilated window is mounted into the building envelope as a conventional window, in which way the building structures do not need special designs for new buildings or reconstructions for existing buildings. The inlet is at the bottom of the window, which is powered by fans to guarantee air circulation. Air from ambient goes through the heat exchanger and ventilated cavity to the indoor or outdoor zone, depending on whether room ventilation is needed or not.

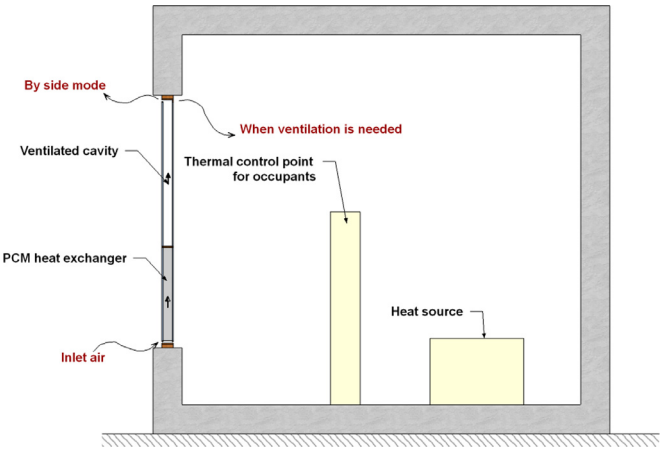


**Fig. 1.** Ventilation widow with PCM heat exchanger.

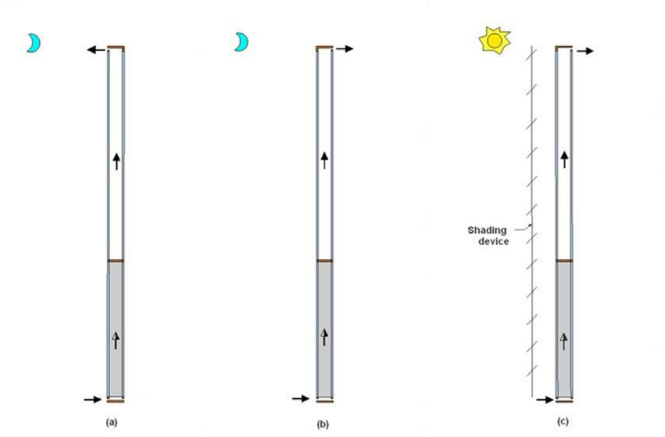


**Fig. 2.** The operation strategies of the PCM ventilation system in summer: (a) night ventilation mode; (b) night free cooling mode; (c) daytime ventilation pre-cooling mode.

Fig. 2 describes the operation strategies of the system. In summer, night ventilation is part of the control strategies. Heat is released from the PCM heat exchanger by cold ambient air during the night. The PCM is reloaded again during daytime by precooling of the outdoor air when ventilation is needed. In the daytime, a shading device is used to prevent the overheating of the system.

Fig. 3 shows the structure of ventilated window. It consists of a ventilated cavity in the upper part and heat exchanger in the lower part. The ventilated cavity is similar to a double glazing window with ventilation in the air gap. The heat exchanger is made of PCM plates located at the same distance from each other to form small air gaps for ventilation. The thickness of the air gap is chosen as 5 mm according to former work [26] in order to guarantee large total PCM volume in the heat exchanger, which is related to large heat storage/release possibility. However, the low thermal conductivity of PCM limits the thickness of PCM plates. As a result, the total amount of PCM is limited and should be optimized.

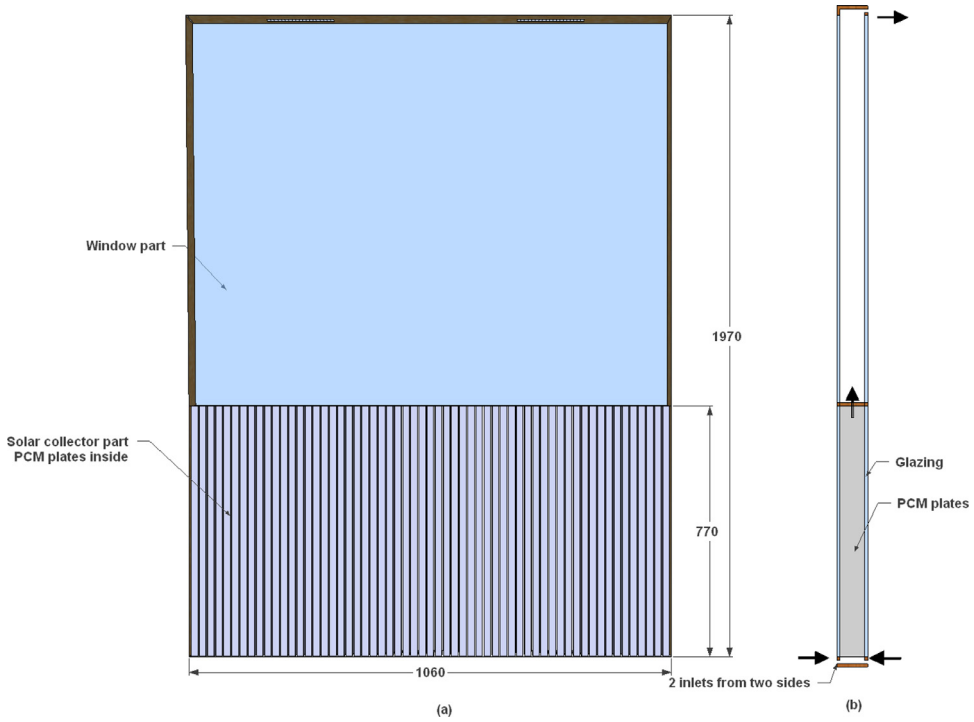


**Fig. 3.** Description of the ventilated window with PCM heat exchanger (a) front view; (b) side view.

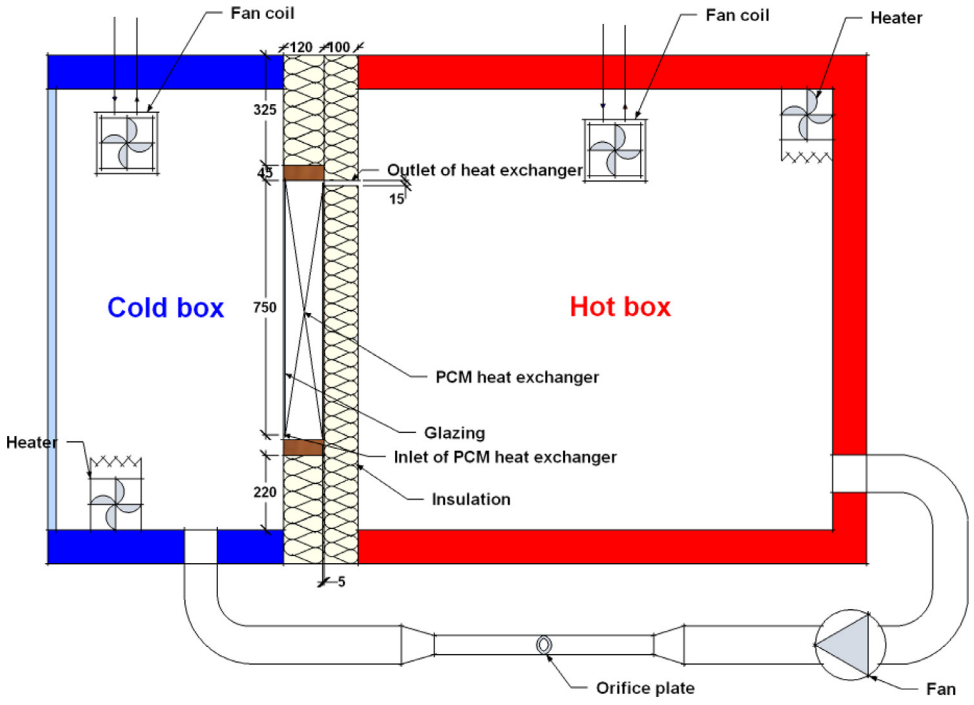


**Fig. 4.** Setup of hot box and cold box for testing the heat exchanger.

## 3. Experimental setup

The heat transfer process of the PCM heat exchanger is studied by full-scale experiments in a hot box and cold box, as seen in Figs. 4 and 5. Both of them are equipped with a water cooling system and an electric heating coil. A proportional–integral–derivative (PID) controller is used to getting the accurate temperature in the two boxes. Moreover, a fancoil provides recirculating airflow at a speed of approximately 0.2 m/s to keep the homogeneous of air temperature in each of the hot box and the cold box. A fan provides an airflow inside the heat exchanger, which creates circulation between the hot box and cold box. The flow rate is measured by an orifice plate with an uncertainty of ±7.5%.

The heat exchanger is mounted in between the two boxes, as shown in Fig. 4. It is supported by insulation boards. It is made of a wooden frame, a glazing cover, and many parallel vertical PCM boards. The distance between any two boards is 5 mm. The details of the PCM plate inside the heat exchanger are shown in

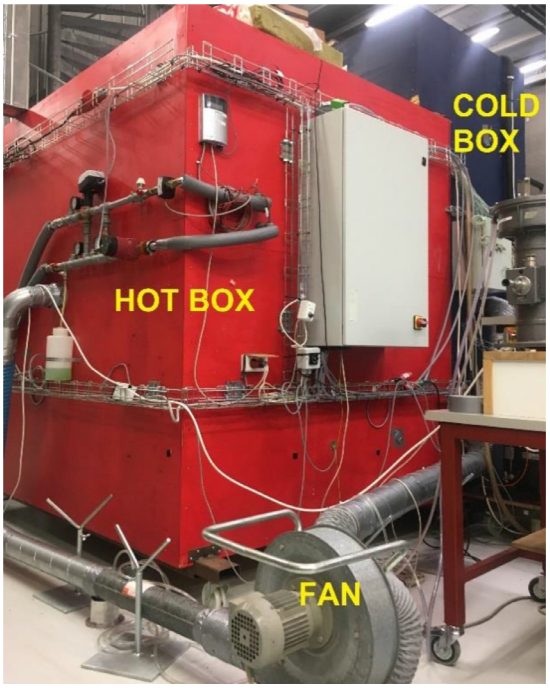


**Fig. 5.** Ventilation system between hot box and cold box.

**Table 1**
Thermal properties of paraffin wax 22.

| Property | Manufacture data (Pure paraffin wax) | DSC measurement (Fiber absorbed PCM) |
|---|---|---|
| Phase change temperature (°C) | 22 | 15–23 |
| Density (kg/m$^3$) | 820 | – |
| Specific heat (kJ/kg/K) | 2.85 | 2.3 |
| Thermal conductivity (W/m/K) | 0.18 | – |
| Latent heat (kJ/kg) | 216 | 117 |
| Max operation temperature (°C) | 400 | – |

Fig. 6. 56K-type thermocouples are used for monitoring the air and PCM temperature, as shown in Fig. 7. The calibration accuracy is ± 0.15 K. The logging time step is 300 s.

The thickness of PCM boards tested in this study is 12.5 mm. The air temperature inside the hot box is kept at 29 ± 1 °C and the cold box is kept at 9 ± 1 °C by PID controller. The flow rate of the fan (same as the flow rate inside the heat exchanger) is 106 m$^3$/h. Firstly, the fan provides airflow from the hot box to the cold box, thus the cold air goes into the inlet of the heat exchanger (in the bottom of the heat exchanger) to cool down the material. After the freezing process is done, the fan direction is changed, resulting in the hot air going into the outlet of the heat exchanger (in the top of the heat exchanger) to melt the material.

The PCM used in the system is paraffin wax with a melting temperature of 22 °C. The PCM is absorbed in a natural fiberboard to form a shape steady plate. The properties of the plate are measured by differential scanning calorimetry (DSC) technology with a heat rate of 0.5 °C/min for freezing and melting processes. Table 1 lists the properties of PCM based on the manufacturer and the DSC measurement.

Fig. 8 shows the heat capacity of the PCM plate in melting and freezing processes from DSC measurement. The total latent heat capacity for the freezing process is 118.8 kJ/kg and for the melting process is 115.2 kJ/kg in the temperature range of [10 °C–30 °C]. The measurement difference is 3.13% between melting and freezing.

Two additional samples are tested in heat rate 0.5 °C/min. The difference for enthalpy in the freezing process is 1.03% and in melting process is 0.16%. The difference of hysteresis between melting and freezing is 0.5 °C–1 °C. This is because the results depend highly on the measurement method.

In this paper, the thermal charge and discharge time is defined as the time period starting from initial condition to the time where the thermal charge or discharge rate is not lower than the fan power. In this work, the fan power is 30 W when the airflow rate is 106 m$^3$/h.

## 4. Methodology

### 4.1. Numerical model

The finite element model is built in COMSOL Multiphysics. The interface of Conjugate Heat Transfer and Laminar Flow multiphysics is used to simulate the coupling between heat transfer and fluid flow. The Laminar Flow interface solves for the conservation of energy, mass, and momentum in fluids, as shown in Eqs. (1)–(3). The flow is assumed incompressible.

$$\rho\frac{\partial \mathrm{u}}{\partial t}+\rho(\mathrm{u}\cdot\nabla)\mathrm{u}=-\nabla p+\mu\nabla^2\mathrm{u}+\rho g\beta\Delta T \tag{1}$$

$$\nabla\cdot\mathrm{u}=0 \tag{2}$$

$$\frac{\partial T}{\partial t}+u\cdot\nabla T=\frac{\lambda}{\rho Cp}\nabla^2 T \tag{3}$$

Where $\rho$ is the density (kg/m$^3$), u is the velocity of air (m/s), $t$ is the time(s), $p$ is the pressure (Pa), $\mu$ is the dynamic viscosity (kg/m/s), g is the acceleration of gravity (m/s$^2$), $\beta$ is coefficient of thermal expansion, $T$ is the temperature(°C), $\lambda$ is the heat conductivity (W/m/ °C), and $Cp$ is the specific heat (kJ/kg).

The Heat Transfer in Solids interface provides features for modeling heat transfer by conduction. The convection is 0 in the fiberboard-based shape steady PCM. The fictive heat capacity based on DSC measurement is used to solve the equation. The energy equation is given in Eq. (4).

$$\frac{\partial T}{\partial t}=\frac{\lambda}{\rho Cp(T)}\nabla^2 T \tag{4}$$

In this work, a 2D model is built for summer case. Half of the PCM plate and half of the air cavity are chosen as the calculation domain, as shown in Fig. 9.

Some hypotheses are necessary to simplify the calculation process. The flow in between the two plates is considered as a 2-dimensional flow to simplify the calculation. The boundary conditions could be simplified as symmetry because of the periodic arrange of PCM plates and air gaps between the plates. Moreover, the thickness of thermal and velocity boundary layers are both considered less than half of the distance between two plates.

Symmetry boundary conditions are considered at x = 0 and x = $(d+e)/2$, as seen in Eqs. (5) and (6).

$$-n\cdot q=0,\ \mathrm{x}=0 \text{ and } \mathrm{x}=(d+e)/2 \tag{5}$$

$$u\cdot n=0,\ \mathrm{x}=(d+e)/2 \tag{6}$$

Thermal insulation boundary conditions are chosen at the top and bottom of the plates, as shown in Eq. (7).

$$-n\cdot q=0, 0<x<d/2, y=0 \text{ and } y=770 \tag{7}$$

The initial boundary conditions are as in Eqs. (8)–(10).

$$T(x,y,0)=T_0 \tag{8}$$

$$T(x,0,t)=T_{inlet}, d/2<x<(d+e)/2 \tag{9}$$

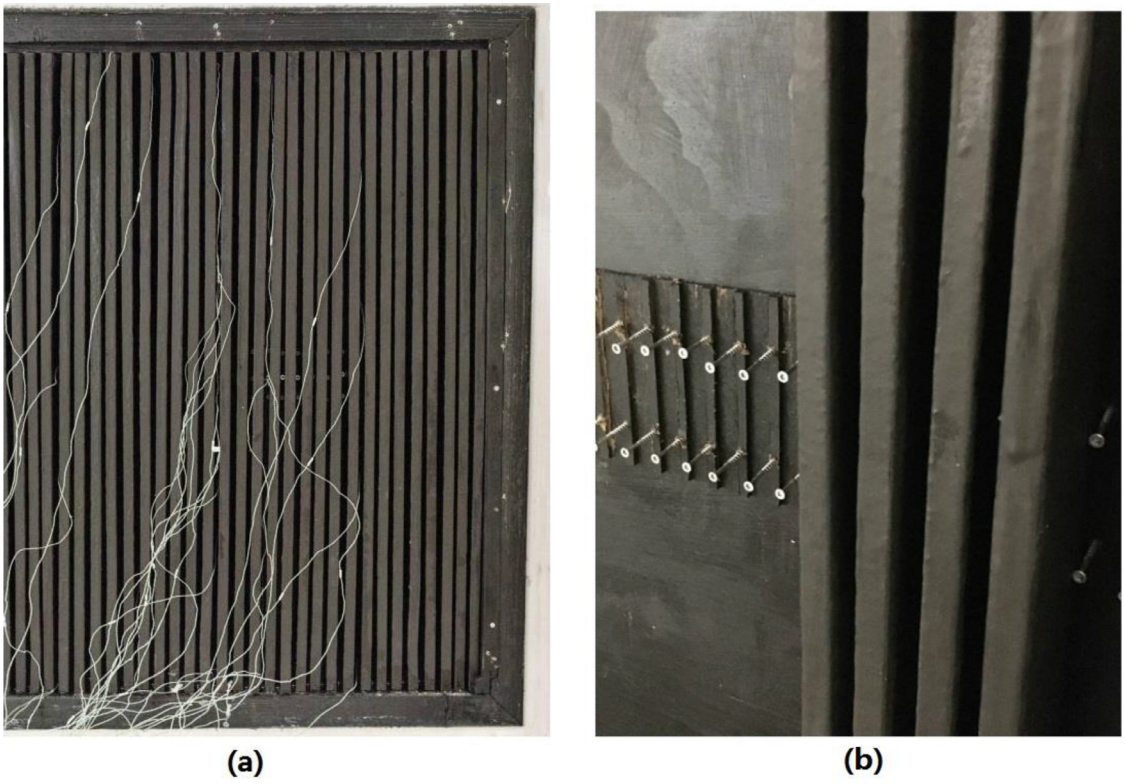


**Fig. 6.** PCM plates inside the wood frame (a) overview; (b) details in installation.

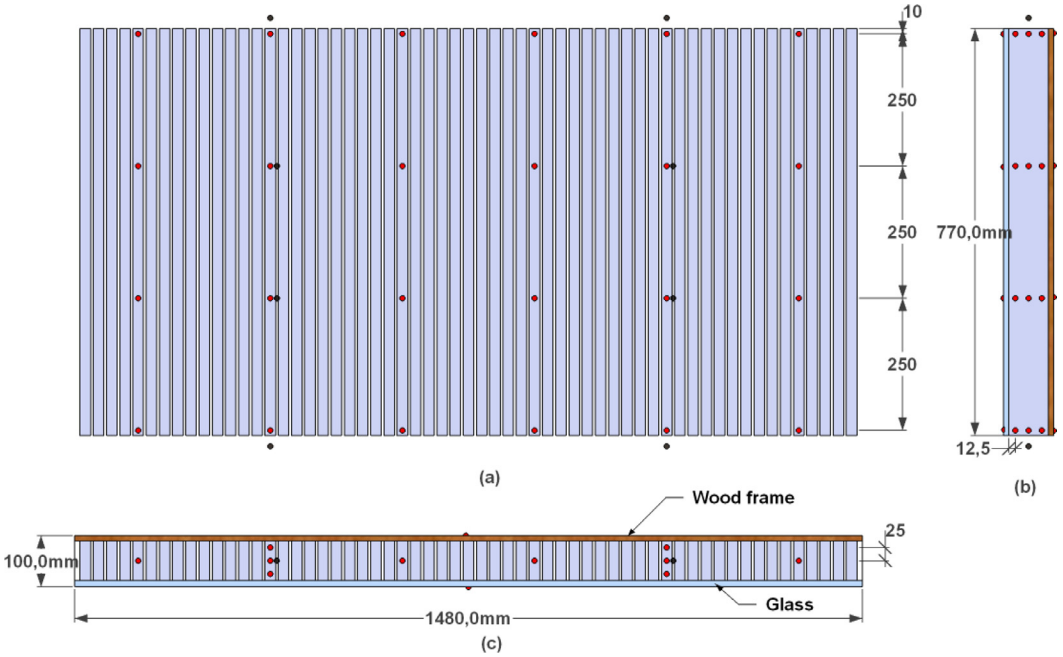


**Fig. 7.** Temperature measurement of the PCM heat exchanger. Red ones represent the PCM temperature measurement points and the black ones are the air temperature measurement points. (a) front view; (b) side view; (c) top view.

$$Q(x, y, t) = 106\mathrm{m}^3/\mathrm{h} \tag{10}$$

The solidification capability of PCM is a key energy performance factor for PCM components in buildings [27]. In this work, a severe summer day in Copenhagen is chosen as the input of the model. Night ventilation mode is analyzed firstly to optimize the PCM plate thickness in the discharging process. Afterwards, the charging process in order to cool down the ventilated air is simulated and the energy saving potential of the heat exchanger is analyzed.

### 4.2. Model validation

Fig. 10 shows the average temperature curves of the PCM plate with different heights in the freezing process. The results from simulation show good consistency with the experimental data. The

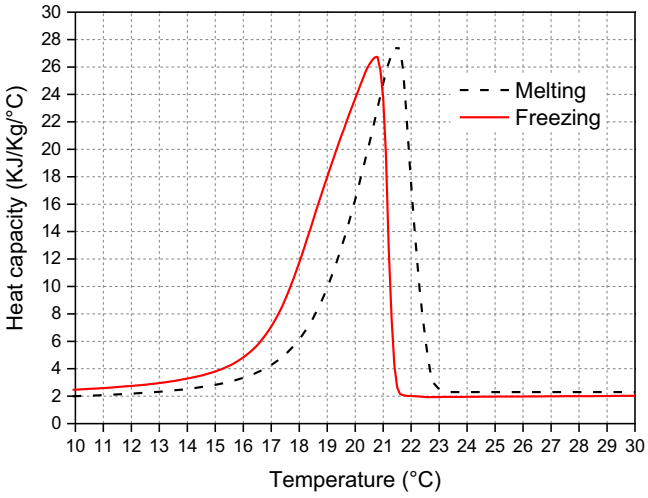


**Fig. 8.** DSC measured heat capacity of the PCM plate in freezing and melting processes.

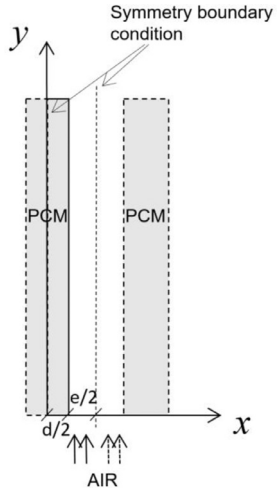


**Fig. 9.** Calculated domain for numerical model.

average error ($\varepsilon$) is 2.38%, which is defined in Eq. (11). The temperature curves at heights 260 mm and 510 mm show better accuracy than in 10 mm and 760 mm. One possible explanation is that the air distribution near the inlet and outlet is complicated in a real situation. For the experiment, the inlet air temperature fluctuates at 8–10 °C because of the limitation of PID controller, which also influences the accuracy of the experiment. As a result, the final value around 7.5 h from the experiment is not convergent at 10 °C. The variations in density between melt and solid can also affect the results.

$$\varepsilon = \left| \frac{\text{Experimental value} - \text{Simulation value}}{\text{Experimental value}} \right| \times 100\% \qquad (11)$$

The phase change start temperature in both simulation results and experimental data is clear. But the end temperature is not. The heat capacity of the material determines the temperature change process. As seen in Fig. 8, the heat capacity used in the model changed sharply around 21.5 °C in the freezing process, but smoothly at the lower temperature. However, the phase change start temperature in the experimental data is higher than the simulation results (except in 10 mm). It is due to the limitation of accuracy in DSC measurement for heat capacity. The uncertainty in the experiment also affects the error between experimental data and simulation results. Nevertheless, the total error is within a reasonable range.

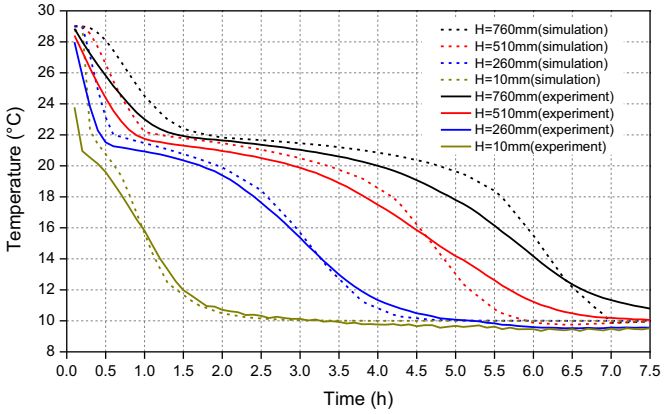


**Fig. 10.** Temperature in the middle of the PCM plate with different heights in the freezing process.

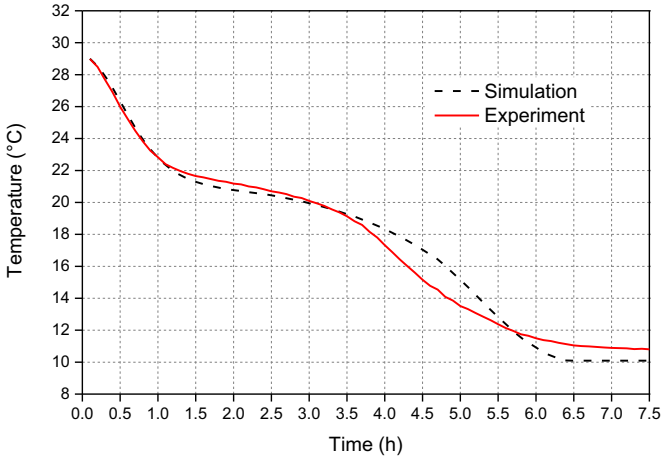


**Fig. 11.** Outlet air temperature in the freezing process.

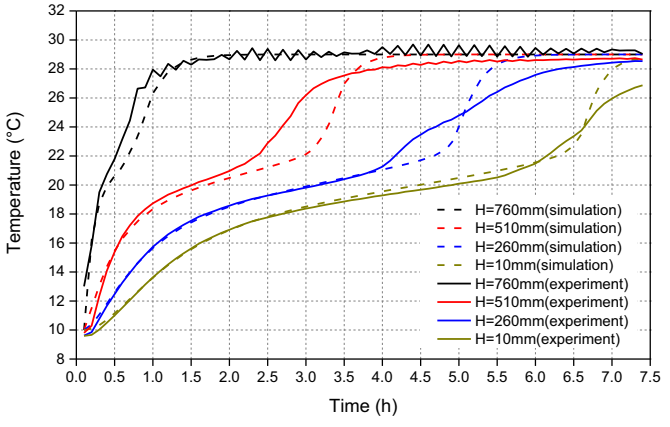


**Fig. 12.** Temperature in the middle of the PCM plate with different heights in the melting process.

Fig. 11 shows the outlet air temperature curves in the freezing process. The error between experimental data and simulation result is 4.41%. The error is higher than the error of PCM temperature, because the air temperature measurement is influenced by more elements such as variability of inlet temperature (8–10 °C) and variability of air flow rate.

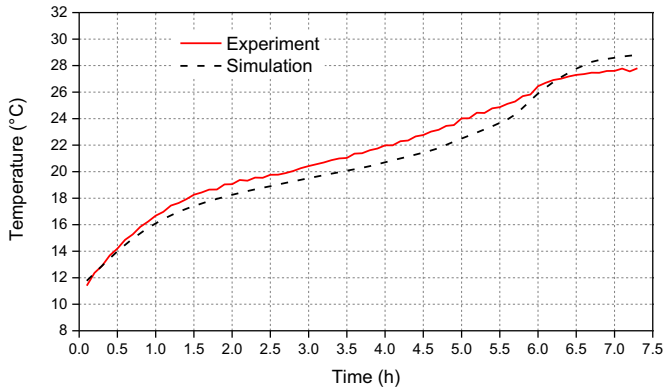


**Fig. 13.** Outlet air temperature in the melting process.

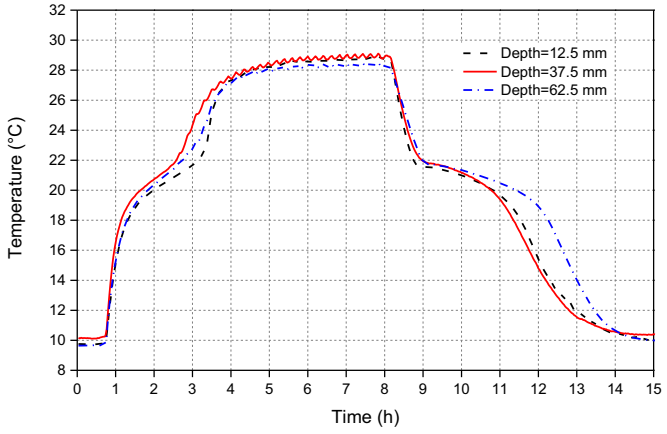


**Fig. 14.** The temperature homogeneity along the length of the PCM plate from experiment.

Fig. 12 shows the average temperature curves of the PCM plate with different heights in the melting process. The results from simulation show good consistency with experimental data. The average error is 4.79%. Similar to Fig. 9, the end temperature of phase change in both simulation results and experimental data is clear. But the start temperature is not. As seen in Fig. 7, the heat capacity used in the model changed sharply around 23 °C in the melting process, but smoothly at the lower temperature. However, the phase change end temperature in experimental data is lower than the simulation results, which means that the hysteresis of melting and freezing processes should be smaller than the DSC measurement results. Nevertheless, the total error is within a reasonable range.

Similarly, Fig. 13 shows the outlet air temperature curves in the melting process. The error between experimental data and simulation results is 3.96%, which is within a reasonable range.

The model output results show good agreement with the experimental data in freezing and melting processes, for both PCM temperature and outlet air temperature. The numerical model is reliable to simulate the heat transfer inside the heat exchanger.

The temperature change along the length of the PCM plate is shown in Fig. 14. The average temperature deviation to the middle point is 2.6% when the depth is 12.5 mm, and 4.2% when the depth is 62.5 mm, which are all in the reasonable range. It is feasible that the numerical model of PCM plates is simplified as 2D.

### 4.3. Climate analysis

Fig. 15 shows the summer outdoor air temperature in Copenhagen. The weather data is obtained from the Design Reference Year based on measurements conducted by DMI to get a typical summer condition [28]. There are 27 days where the maximum outdoor air temperature is above 23 °C. There are 194 h in which the outdoor air temperature is above 23 °C in those 27 days, which are necessary for applying ventilation pre-cooling. Among the days when ventilation pre-cooling is necessary, the minimum temperature is all below 18.1 °C, and 11 days of them the minimum temperature during the night are below 14 °C, which are suitable for the application of night ventilation.

A severe summer day in Copenhagen is chosen as the model input. As shown in Fig. 16, the average air temperature from 0:00 to 4:00 is around 14 °C, which is suitable for night ventilation. The air temperature from 11:00 to 15:00 is higher than 26 °C and air conditioning is needed to remove the cooling load from the ventilated fresh air. The control strategy is designed accordingly. The fan is turned on from 0:00 to 4:00, and the system is in night ventilation mode. It is turned on again from 11:00 to 15:00 in the daytime ventilation pre-cooling mode.

## 5. Results

### 5.1. Summer night ventilation mode

Night ventilation for PCM solidification is analyzed based on some assumptions. The ventilation starts from a point where the PCM system is fully charged with heat. The system needs to be discharged by the low-temperature ambient air. The cold air is ventilated from the bottom of the heat exchanger and into the air gaps between the PCM plates. The ventilation is stopped when the PCM is fully cooled down or the ambient air temperature is too high to remove heat from the PCM. The inlet air temperature is set as 14 °C as the average temperature during the midnight observed in Copenhagen is around 14 °C.

The thickness of PCM plates inside the heat exchanger should be chosen in a way that both the heat transfer amount and response time are optimized. The PCM utilization rate is also an important element to decide the right design of PCM heat exchanger and save material cost.

4 models with different plate thicknesses are calculated and compared. Table 2 shows the differences between the models.

Fig. 17 shows the outlet air temperature of the heat exchanger in the night ventilation mode. For the first two hours, the difference of outlet air temperature for different plate thicknesses is not so big. It is the sensible heat being released from the PCM to the ventilated air, and it is quite small in comparison with latent heat. A slower temperature change for all the cases is observed from around 21 °C until 14 °C, during which period the PCM in the heat exchanger is going through a phase change process and the released energy density is relatively high. Moreover, the system response time for the 5 mm plate thickness is relatively short and for 20 mm is relatively long.

Fig. 18 illustrates the heat release from the heat exchanger with different plate thicknesses. For 0–5 h discharge time, the cold storage amounts are similar for 10, 15, and 20 mm plate thickness. A big difference is shown for 5 mm plate thickness after around 3.6 h. For a specific summer case, the discharge time is limited by the outdoor climate as well as fan energy consumption. A PCM heat exchanger with 10 mm plate thickness is recommended, and the discharge time is recommended as 4–5 h to maximize the cold storage to the system volume. For 10 mm plate thickness, the cold storage ability is similar to 20 mm plate thickness within the recommended discharge time. However, the cost of material in the heat exchanger decreased by 16.87%. For the cases in which the efficient discharge time is shorter (0–3.6 h) because of the climate limitation, the recommended plate thickness is 5 mm. The cost of

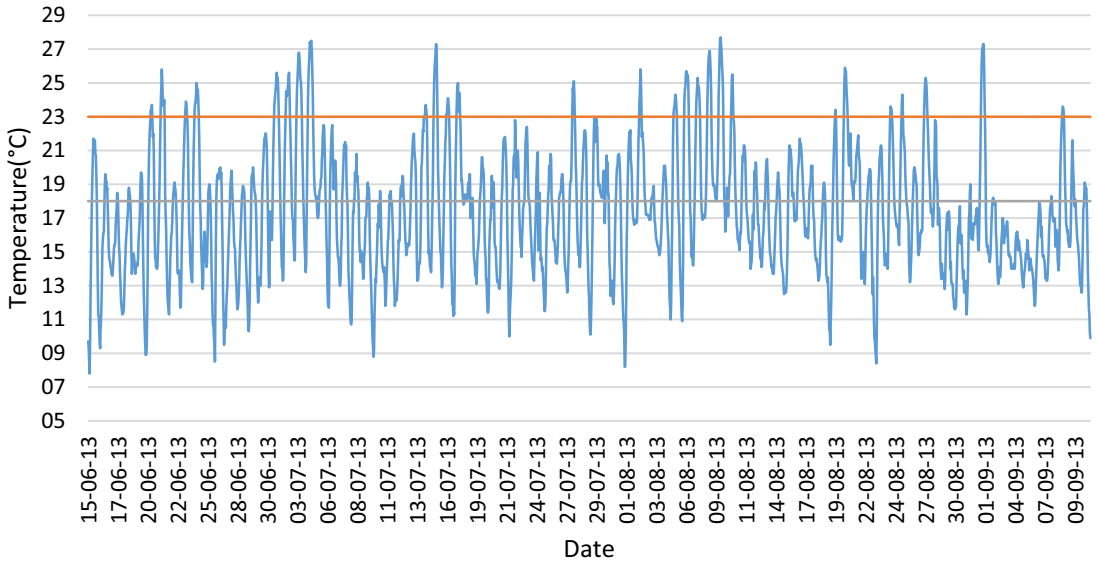


**Fig. 15.** Summer outdoor air temperature in Copenhagen from the Design Reference Year.

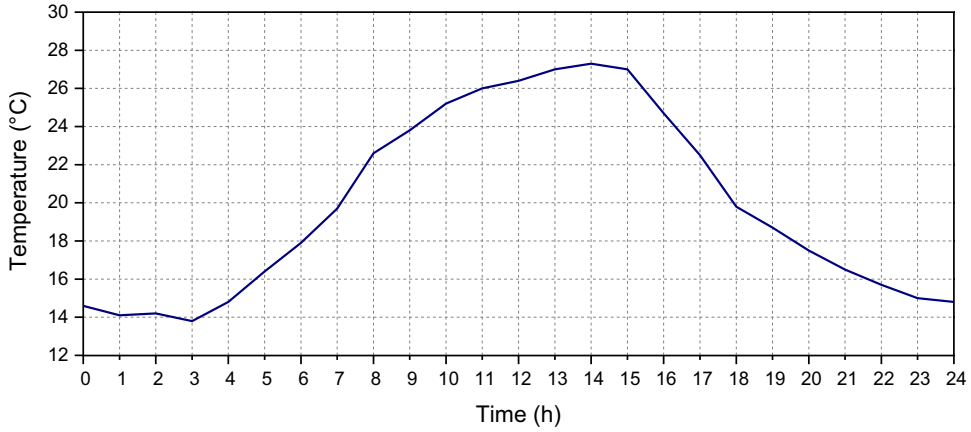


**Fig. 16.** Outdoor air temperature (07.15) for a severe summer day in Copenhagen.

**Table 2**
Models of heat exchanger with different PCM plate thicknesses.

| d (mm) | e (mm) | Air velocity (m/s) | Number of plates in total | Plate depth (mm) | Air flow rate ($m^3$/h) | Total PCM surface area ($m^2$) | Total PCM volume ($m^3$) |
|---|---|---|---|---|---|---|---|
| 5 | 5 | 0.74 | 106 | 75 | 106 | 22.30 | 0.052 |
| 10 | | 1.09 | 70 | | | 15.69 | 0.069 |
| 15 | | 1.48 | 53 | | | 12.62 | 0.078 |
| 20 | | 1.78 | 42 | | | 10.58 | 0.083 |

material in the heat exchanger decreased by 37.35% compared to 20 mm plate thickness.

### 5.2. Pre-cooling potential

The whole heat transfer process for discharge and charge together is complicated because of the hysteresis between the melting and freezing processes. The temperature change may not be consecutive if the PCM does not go through the full phase change process. For the modeling of the charging process, the difficulty lies in the definition of the initial values from the former process.

Fig. 19 describes the enthalpy transfer when the PCM cools down first and then goes through the melting process. The enthalpy curves for melting and freezing are based on the DSC measurement. Process 2 is the enthalpy transition between freezing and melting. It is not horizontal because of the change of the sensible heat. It is parallel to the beginning of the freezing process. The recharged heat and the initial temperature of melting process could be confirmed in this way. Once the initial temperature of melting process is confirmed, the corresponding Cp in melting process could be determined, as shown in Fig. 20.

The enthalpy and heat capacity transitions are set in the numerical model. Two models are calculated, with a plate thickness of 5 mm and 10 mm respectively. The outdoor air temperature in the severe summer day in Copenhagen is used as model input. The time for night ventilation mode is 00:00–04:00. The time for ventilation pre-cooling mode is 11:00–15:00.

Fig. 21 shows the cooling ability of the heat exchanger in ventilation pre-cooling mode. The average temperature difference between the ambient air and outlet air is 6.5 °C from 11:00 to 15:00 when the plate thickness is 10 mm. The average temperature differ-

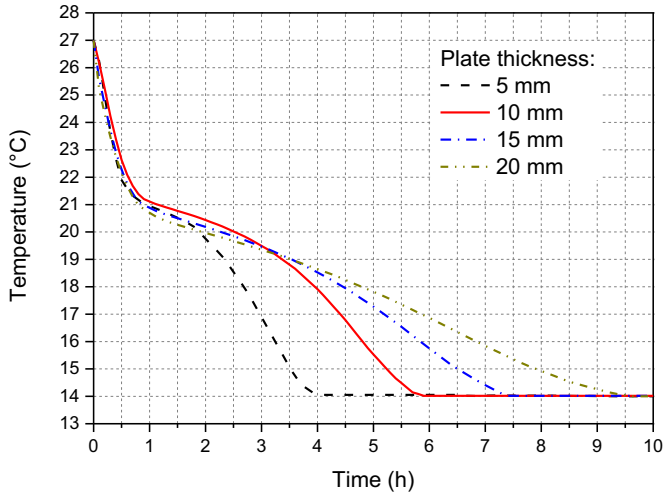


**Fig. 17.** Outlet air temperature of the heat exchanger with different plate thicknesses.

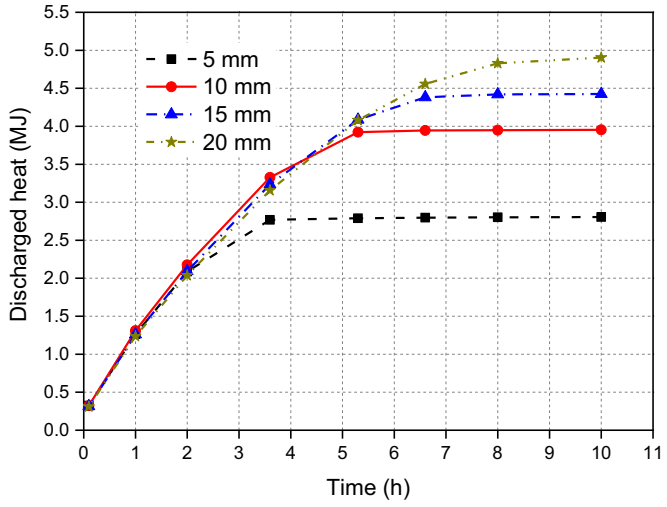


**Fig. 18.** Discharged heat from the heat exchanger with different plate thicknesses.

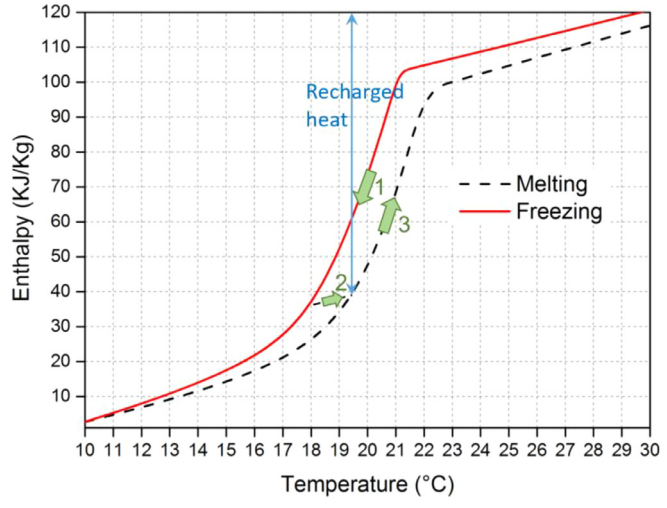


**Fig. 19.** Enthalpy in relation to temperature transition.

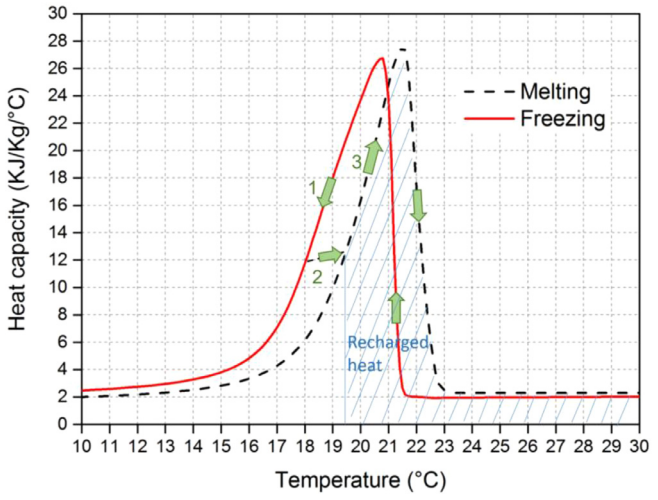


**Fig. 20.** Heat capacity in relation to temperature transition.

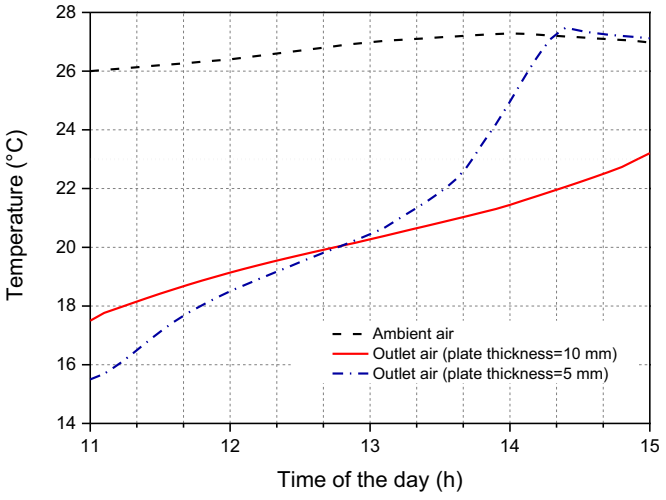


**Fig. 21.** Cooling ability of the heat exchanger in ventilation pre-cooling mode.

ence between the ambient air and outlet air is 7.11 °C from 11:00 to 13:48 when the plate thickness is 5 mm.

The discharge efficiency ($\zeta$) is calculated by the ratio between the heat storage in pre-cooling mode and the heat release in the night ventilation mode, which is in Eq. (12).

$$\zeta = \frac{\rho_{air} q C p_{air} \int_{t_m}^{t_n} |T_{ambient} - T_{inlet}| dt}{\rho_{air} q C p_{air} \int_{t_i}^{t_j} |T_{outlet} - T_{inlet}| dt} \quad (12)$$

Where $t_m = 0$ h, $t_n = 4$ h, $t_i = 11$ h, $t_j = 15$ h.

When the plate thickness is 10 mm, the discharged heat in night ventilation mode is 3.55 MJ in this work. The charged heat for air pre-cooling mode is 3.19 MJ. The discharge efficiency of the heat exchanger is 89.85%. The effect time (the outlet air temperature lower than 23 °C) is 3.9 h. When the plate thickness is 5 mm, the discharged heat in night ventilation mode is 2.79 MJ. The charged heat for air pre-cooling mode is 2.52 MJ. The discharge efficiency of the heat exchanger is 90.32%. The effect time is 2.7 h.

In comparison, a heat exchanger with 5 mm plate thickness has a shorter discharge time and shorter charge time. It can be cooled down faster and recharged faster, which is good for the climate when the outdoor air temperature suitable for night ventilation is short, such as hot summer climate (but such climate always has long hours in which cooling is needed during daytime). A heat exchanger with 10 mm plate thickness has longer discharge time and

charge time. There is more stability of outlet air temperature in the ventilation pre-cooling mode as well.

## 6. Conclusions

This paper presents a new window application for pre-cooling of ventilation air using a PCM heat exchanger. In summer, the PCM heat exchanger is discharged by night ventilation, and recharged by high-temperature ambient air in pre-cooling mode.

The design and optimization processes of the heat exchanger are conducted by means of numerical modeling, which is verified by full-scale experiments. The nonlinear properties and hysteresis of PCM are set in the model. The hysteresis of PCM used in the model is slightly overvalued by DSC measurement, but the deviation from the experiment lies within a reasonable range.

The numerical works are conducted based on a severe summer day in Copenhagen. Results show that in night ventilation mode, the increase in PCM plate thickness does not have a big influence on the outlet air temperature and discharged heat in the first hours of the discharge process. 10 mm plate thickness for the heat exchanger is recommended when 4–5 h discharge time available during the night, which saves 16.87% material cost with similar discharged heat (compared with the heat exchanger with 20 mm plate thickness). 5 mm plate thickness for the heat exchanger is recommended when there is only 0–3.6 h discharge time available during the night, which saves 37.35% material cost with similar discharged heat.

In ventilation pre-cooling mode, the saved energy from the heat exchanger with 10 mm plate thickness is 3.19 MJ/day. The discharge efficiency of the heat exchanger is 89.85%.The effect pre-cooling time is 3.9 h. The saved energy from the heat exchanger with 5 mm plate thickness is 2.52 MJ/day. The discharge efficiency of the heat exchanger is 90.32%. The effect pre-cooling time is 2.7 h.

In the case study in Copenhagen, the heat exchanger with 10 mm plate thickness has more stable pre-cooled air temperature in longer effective pre-cooling time with a higher energy saving amount than 5 mm, and the discharge can be fulfilled during the night in this climate. Nevertheless, the heat exchanger with 5 mm plate thickness has a fast thermal response, which is good for the climate where the duration of outdoor air temperature suitable for night ventilation is short.

New methods to get more accurate PCM heat capacity is essential for future works. It is also necessary to conduct more climate analyses to verify the optimized results. In the next stage, the studies will include the feasibility of applying the PCM heat exchanger for solar energy storage in winter and its air pre-heating effect.

## Acknowledgment

This work is carried out within the EU Horizon 2020 research and innovation programme under grant agreement NO. 768576 (ReCO2ST). Moreover, the first author gratefully acknowledge the financial support from the Chinese Scholarship Council (CSC No. 201606050118).

## References

[1] M. Iten, S. Liu, A. Shukla, A. Shukla, A review on the air-PCM-TES application for free cooling and heating in the buildings, Renew. Sustain, Energy Rev. 61 (2016) 175–186, doi:10.1016/j.rser.2016.03.007.
[2] H. Akeiber, P. Nejat, M.Z.A. Majid, M.A. Wahid, F. Jomehzadeh, I. Zeynali Famileh, J.K. Calautit, B.R. Hughes, S.A. Zaki, A review on phase change material (PCM) for sustainable passive cooling in building envelopes, Renewable Sustainable Energy Rev. 60 (2016) 1470–1497, doi:10.1016/j.rser.2016.03.036.
[3] E. Osterman, V.V.V. Tyagi, V. Butala, N.A.A. Rahim, U. Stritih, Review of PCM based cooling technologies for buildings, Energy Build. 49 (2012) 37–49, doi:10.1016/j.enbuild.2012.03.022.
[4] H. Johra, P. Heiselberg, Influence of internal thermal mass on the indoor thermal dynamics and integration of phase change materials in furniture for building energy storage: a review, Renewable Sustainable Energy Rev. 69 (2017) 19–32, doi:10.1016/J.RSER.2016.11.145.
[5] V.A. Aroul Raj, R. Velraj, Review on free cooling of buildings using phase change materials, Renewable Sustainable Energy Rev. 14 (2010) 2819–2829, doi:10.1016/j.rser.2010.07.004.
[6] M. Pomianowski, P. Heiselberg, R. Lund Jensen, Dynamic heat storage and cooling capacity of a concrete deck with PCM and thermally activated building system, Energy Build. 53 (2012) 96–107, doi:10.1016/j.enbuild.2012.07.007.
[7] G. Diarce, A. Urresti, A. García-Romero, A. Delgado, A. Erkoreka, C. Escudero, Á. Campos-Celador, Ventilated active façades with PCM, Appl. Energy 109 (2013) 530–537, doi:10.1016/j.apenergy.2013.01.032.
[8] A. De Gracia, L. Navarro, A. Castell, Á. Ruiz-Pardo, S. Álvarez, L.F. Cabeza, Thermal analysis of a ventilated facade with PCM for cooling applications, Energy Build. 65 (2013) 508–515, doi:10.1016/j.enbuild.2013.06.032.
[9] L. Karlsen, P. Heiselberg, I. Bryn, H. Johra, Solar shading control strategy for office buildings in cold climate, Energy Build. 118 (2016) 316–328, doi:10.1016/j.enbuild.2016.03.014.
[10] P. Heiselberg, O. Kalyanova, CLIMAWIN: Technical Summary Report, vol. 160, 2013, p. 92 http://vbn.aau.dk/files/203815355/CLIMAWIN_Technical_Summary_Report.pdf.
[11] L. Fan, J.M. Khodadadi, Thermal conductivity enhancement of phase change materials for thermal energy storage: a review, Renewable Sustainable Energy Rev. 15 (2011) 24–46, doi:10.1016/J.RSER.2010.08.007.
[12] W.M. Huang, Y. Zhao, C.C. Wang, Z. Ding, H. Purnawali, C. Tang, J.L. Zhang, Thermo/chemo-responsive shape memory effect in polymers: a sketch of working mechanisms, fundamentals and optimization, J. Polym. Res. 19 (2012) 9952, doi:10.1007/s10965-012-9952-z.
[13] Heat and cold storage with PCM, Springer Berlin Heidelberg, Berlin, Heidelberg, 2008, doi:10.1007/978-3-540-68557-9.
[14] Modeling phase change materials behavior in building applications: comments on material characterization and model validation, Renewable Energy 61 (2014) 132–135, doi:10.1016/J.RENENE.2012.10.027.
[15] R. Baetens, B.P. Jelle, A. Gustavsen, Phase change materials for building applications: a state-of-the-art review, Energy Build. 42 (2010) 1361–1368, doi:10.1016/j.enbuild.2010.03.026.
[16] F. Kuznik, J. Virgone, Experimental investigation of wallboard containing phase change material: Data for validation of numerical modeling, Energy Build. 41 (2009) 561–570, doi:10.1016/J.ENBUILD.2008.11.022.
[17] A. Buonomano, G. De Luca, U. Montanaro, A. Palombo, Innovative technologies for NZEBs: an energy and economic analysis tool and a case study of a non-residential building for the mediterranean climate, Energy Build. 121 (2016) 318–343, doi:10.1016/j.enbuild.2015.08.037.
[18] J. Virgone, A. Trabelsi, 2D Conduction Simulation of a PCM Storage Coupled with a Heat Pump in a Ventilation System, Appl. Sci. 6 (2016) 193. http://dx.doi.org/10.3390/app6070193.
[19] Verification and validation of EnergyPlus phase change material model for opaque wall assemblies, Build. Environ. 54 (2012) 186–196, doi:10.1016/J.BUILDENV.2012.02.019.
[20] Establishment and experimental verification of PCM room's TRNSYS heat transfer model based on latent heat utilization ratio, Energy Build. 84 (2014) 287–298, doi:10.1016/J.ENBUILD.2014.07.082.
[21] Numerical modelling and thermal simulation of PCM–gypsum composites with ESP-r, Energy Build. 36 (2004) 795–805, doi:10.1016/J.ENBUILD.2004.01.004.
[22] K. Biswas, J. Lu, P. Soroushian, S. Shrestha, S. Shrestha, Combined experimental and numerical evaluation of a prototype nano-PCM enhanced wallboard, Appl. Energy. 131 (2014) 517–529, doi:10.1016/j.apenergy.2014.02.047.
[23] M. Liu, W. Saman, F. Bruno, Validation of a mathematical model for encapsulated phase change material flat slabs for cooling applications, Appl. Therm. Eng. 31 (2011) 2340–2347, doi:10.1016/j.applthermaleng.2011.03.034.
[24] C. Hasse, M. Grenet, A. Bontemps, R. Dendievel, H. Sallée, Realization, test and modelling of honeycomb wallboards containing a Phase Change Material, Energy Build. 43 (2010) 232–238, doi:10.1016/j.enbuild.2010.09.017.
[25] P. Lamberg, R. Lehtiniemi, A.-M. Henell, Numerical and experimental investigation of melting and freezing processes in phase change material storage, Int. J. Therm. Sci. 43 (2004) 277–287, doi:10.1016/j.ijthermalsci.2003.07.001.
[26] H. Yue, H. Per, Thermal performance of ventilated solar collector with energy storage containing phase change material, 38th AIVC Conf. "Ventilating Heal. Low-Energy Build, 2017 http://www.aivc.org/resource/thermal-performance-ventilated-solar-collector-energy-storage-containing-phase-change?volume=37270 (accessed November 30, 2017).
[27] J. Kośny, PCM-Enhanced Building Components, Springer International Publishing, Cham, 2015, doi:10.1007/978-3-319-14286-9.
[28] BSim - Climate data, (n.d.). http://sbi.dk/bsim/Pages/Klimadata.aspx#TRY (accessed November 16, 2017).